Date of publication xxxx 00, 0000, date of current version xxxx 00, 0000.

Digital Object Identifier 10.1109/ACCESS.2020.DOI

Upper-Limb Kinematic Parameter Estimation and Localization using a Compliant Robotic Manipulator

FRANCISCO J. RUIZ-RUIZ[1], JUAN M. GANDARIAS[2], (Member, IEEE), FRANCISCO PASTOR[1], AND JESÚS M. GÓMEZ-DE-GABRIEL[1], (Member, IEEE)

[1]Robotics and Mechatronics Group, University of Malaga, Spain (e-mail: {fjruiz2, fpastor, jesus.gomez}@uma.es)
[2]HRI[2] Lab, Istituto Italiano di Tecnologia (IIT), 16163 Genoa, Italy (e-mail: juan.gandarias@iit.it)

Corresponding author: Francisco J. Ruiz-Ruiz (e-mail: fjruiz2@uma.es).

*This work was supported by the Spanish projects UMA CEIATECH-23, RTI2018-093421-B-I00, FEDER 2018 EQC2018- 004299-P, and the University of Málaga.

ABSTRACT Assistive and rehabilitation robotics have gained momentum over the past decade and are expected to progress significantly in the next years. Although relevant and promising research advances have contributed to these fields, existing challenges regarding intentional physical contact with humans are to be faced. Despite being a fundamental operation in assistive and rehabilitation tasks, there is an evident lack of works related to robotic manipulators that intentionally manipulate human body parts. Besides, existing solutions involving end-effector robots are not based on accurate knowledge of human limbs' dimensions and current configuration. This knowledge, which is essential for safe human–limb manipulation, depends on the grasping location and human kinematic parameters. This paper addresses the upper limb manipulation challenge and proposes a pose estimation method using a compliant robotic manipulator. To the best of our knowledge, this is the first procedure in tackling this challenge. A kinesthetic-based approach enables estimating the human arm's kinematic parameters without integrating external sensors. The estimation method relies only on proprioceptive data obtained from a collaborative robot with a Cartesian impedance-based controller to follow a compliant trajectory that depends on human arm kinodynamics. The human arm model is considered as a 2-degree of freedom (DoFs) kinematic chain. Thus, prior knowledge of the arm's behavior and an estimation method enables estimation of the kinematic parameters. Two estimation methods are implemented and compared: i) Hough Transform (HT); ii) Least Squares (LS). Besides, a resizable, sensorized dummy arm is designed for experimental validation of the proposed approach. Outcomes from six experiments with different arm lengths demonstrates the repeatability and effectiveness of the proposed methodology, which can be used in several rehabilitation robotic applications.

INDEX TERMS Human–Robot Interaction, Motion Analysis, Robot Motion, Assistive Robotics

I. INTRODUCTION

ASSISTIVE robots can be defined as devices equipped with sensory, perceptive, and cognitive capabilities to physically help disabled or elderly people in daily-life activities, thus circumventing the need for an attendant [1]. Typical existing applications involving this technology include activities that do not require high levels of physical interactions, such as feeding [2] or dressing [3]. However, the ability to facilitate tasks that involve high levels of physical interaction, such as climbing stairs or standing up from a bed or chair [4], relocating limbs [5], object handovers [6], and stabilizing limb motions [7], is also desired in assistive robots.

These physical assistance devices can also be employed in other fields, such as rehabilitation robotics, which has gained importance in recent years [8]. This field of robotics offers multiple benefits by improving treatment quality in terms of repeatability and efficiency and providing an objective approach to evaluate patients' progress [9]–[12].

One of the main challenges in physical robotic attendance and rehabilitation is the manipulation of human limbs [13]–[15]. In previous studies, this challenge has been tackled using two main approaches: exoskeletons and end-effector devices. Exoskeletons have been extensively studied and used for both assistance and rehabilitation purposes. These

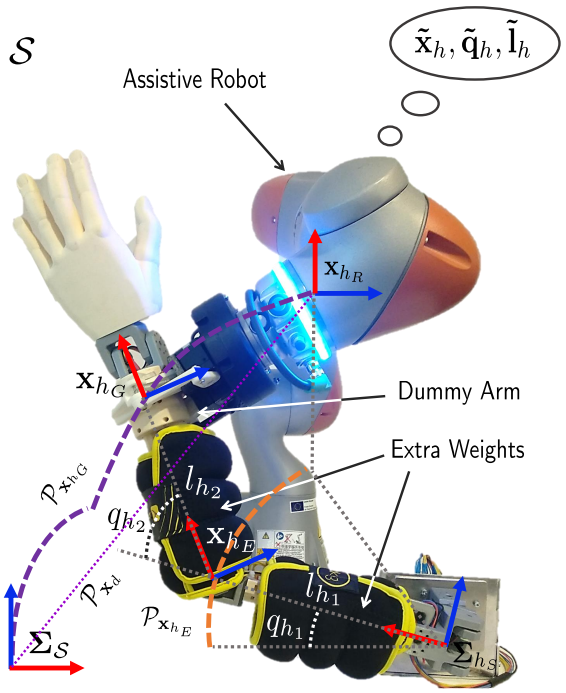

FIGURE 1. Illustration of the problem tackled in this work: A compliant robot manipulating a 3D-printed dummy arm that simulates the behavior of a human arm. Due to the compliance of the Cartesian impedance controller, the robot motion adapts to the kinodynamics of the dummy arm, modifying the end-effector trajectory, and allowing the estimation of the kinematic parameters. The XYZ-RGB convention has been applied in all reference frames. A full description of the parameters can be found in Section II.

systems are wearable devices designed for multiple purposes. Some of these applications include, but are not limited to help patients in their daily tasks (e.g., suppressing upper limb tremors in people with neurological damage [16]), assist people to handle heavy loads [17], or rehabilitation (e.g., as hand and wrist rehabilitation robots described in [18] and [19]). However, they are usually heavy, obtrusive, and hard to wear. In contrast, end-effector systems, although bulky, tend to be multipurpose. This solution can be implemented using collaborative robot arms (Cobots), sensitive manipulators, or industrial manipulators with external force/torque sensors [20], [21]. One of the main advantages is that they are not attached to the human body. Hence, the same system can be used for multiple tasks, especially if they are mounted on a mobile platform [22]. Regarding rehabilitation applications, end-effector robots are thought to be used under a therapist's supervision, and they have also been successfully used for upper limb tremor suppression [7]. Apart from these two approaches, a few ad-hoc solutions based on custom-designed devices with unique mechanical configurations have also been considered [23], [24]. One of the main advantages of these solutions is that they provide more efficient or safer functionality in specific tasks [25].

This work focuses on the application of compliant, end-effector manipulator systems for rehabilitation tasks. Sensitive manipulators include joint torque sensors that can be used to provide compliant control schemes in the task space. Cartesian impedance control in robots used for human interactions enables the robot to adapt to physical contact with the user. In this respect, low impedance ensures more compliant robot behavior but can cause poor task performance in terms of movement accuracy and precision. In contrast, a high impedance improves the programmed task's performance but can compromise user safety. Nevertheless, in the works cited before, the robotic systems never adopt an active manipulative role. I.e., the robots do not directly manipulate the human limb, but adapt to the motion intended by the human. During direct manipulation of human body parts, using a stand-alone compliant controller does not ensure safety, and more information is needed. In this respect, an accurate kinodynamic model of the human subject and real-time monitoring of the joint pose of the subject lead to several improvements in performance, safety and precision.

Existing approaches include visual methods for estimating human posture [26], [27]. However, due to several limitations (e.g., camera placement, illumination settings, or occlusions), such methods are not accurate and robust enough for daily life activities with critical safety restrictions. To overcome this problem, a combination of optical [28], [29] and inertial [30], [31] sensors is usually employed. These solutions involve computationally expensive algorithms that must be executed concurrently with the application. Consequently, synchronization between the two systems is essential for accomplishing the task.

A different approach consists of the use of proprioceptive information. A robot can obtain the human subject kinodynamic model from the resultant trajectories of the physical Human–Robot Interaction (pHRI) task. Based on this concept, a method that estimates the link weights in human upper limbs to compensate for the gravitational forces of exoskeletons has recently been presented [32]. Laitenberger *et al.* proposed a method to estimate the parameter values using offline external tools [33]. Moreover, recent developments in robot sensing for pHRI include the use of underactuated grippers equipped with tactile sensing and kinesthetic (position) perception to improve their knowledge of the grasped objects [34], and estimation of the roll angle of the grasped human forearm with an underactuated gripper [5]. Based on the same principle, the compliant robot's resulting trajectories during the manipulation of a human limb can be used as individual-specific data to estimate the limb's kinematic parameters and poses.

This study contributes to the human-limb robotic manipulation problem tackling the challenge of upper limb parameter estimation with a commercial robot arm, using kinesthetic information only. In this paper, we propose a novel approach that only requires a simple ascendant motion to estimate a passive person's arm's kinematic parameters. To the best of the authors' knowledge, this study represents the first and only work in this domain. The proposed method allows for estimating the human arm's kinematic model without the need for external sensors (e.g., cameras, mocaps). Motion

planning algorithms can then be used with the estimated model in multiple assistive and rehabilitation applications that require upper limb manipulation. The estimated parameters include the distance from the grasping location to the elbow, the distance between the elbow and shoulder axes (humerus length), and the elbow and shoulder poses. This task requires a manipulator robot with Cartesian compliance control, a suitable gripper, and real-time position feedback. When no visual methods are used, the initial grasping of the human forearm is performed with the help of a human supervisor. Once the attachment is done, the method is fully autonomous and does not require any supervision. To validate our approach, a 3D-printed, customizable, sensorized anthropomorphic arm is used. The dummy arm has 6-DoF and similar lengths and masses to the human arm. Besides, it integrates joint sensors that provide ground-truth data.

The remainder of this paper is organized as follows: In Section II, we present the problem, its formulation, and constraints. Section III describes the proposed method. In Section IV, the experiments carried out to evaluate the system's performance under different kinodynamic conditions are presented. In Section V, we discuss the experimental results and the limitations of the proposed methodology. Finally, Section VI presents the conclusions and possible lines of future research.

II. PROBLEM STATEMENT

The challenge described above is simplified by assuming that the human arm is extended with the forearm section lying on a surface, as typically observed in various rehabilitation tasks [35]–[37]. Considering this scenario illustrated in Fig. 1, a compliant robot grasps the arm to manipulate it in a specific way based on the desired task. During the manipulation, the robot may perform motions in the human-arm task space causing the arm to reach dangerous configurations in the joint space and, therefore, injuries to the subject. Examples of unsafe movements include those that exceed the joint range or cause the elbow to hit nearby surfaces (e.g., floor, bed, stretcher), leading to possible physical injury for a vulnerable person (elderly, patient, or victim).

A. APPROACH

The proposed approach involves developing a method to identify the kinematic parameters of a human upper limb for pose estimation and safe manipulation with a compliant robot, considering the robot does not have any previous information about these parameters. This method is based on implementing an estimation trajectory before the desired assistive or rehabilitation task. Once the motion is initiated, the robot can use an estimated kinematic model to limit the workspace and plan the motions according to the task requirements and safety restrictions.

A schematic of the problem is shown in Fig. 1, where all the geometric elements are represented in the human sagittal plane ($\mathcal{S}$). The subscript h refers to the human arm, with $\mathbf{x}_{h_G}$, $\mathbf{x}_{h_E}$, $\mathbf{x}_{h_S} \in \mathbb{R}^3$ representing the pose (position $\in \mathbb{R}^2$ and orientation $\in \mathbb{R}$) of the grasping point, elbow, and shoulder, respectively. For clarity, the XYZ-RGB convention is used in all the figures in this paper. Hence, the axis labels of the reference frames are omitted.

Another assumption involved in our proposal is that the human subject is considered as entirely passive (i.e., an unconscious person or a relaxed, collaborative patient) during the estimation motion. In a real-world scenario, a supervisor or therapist should ask the patient to remain still while the robot is performing the estimation trajectory. Hence, the torques at the human arm joints are null ($\boldsymbol{\tau}_h = 0$). Therefore, all wrenches applied to the human arm originate from the gravitational forces of the arm and the motion of the robot manipulator. The robot has an impedance-based controller (explained in Section III-B), which ensures compliant motion when the robot moves the human arm in $\mathcal{S}$ while restricting the motion out of this plane. This compliance causes the trajectory of the end-effector to change due to the dynamic effects and kinematic constraints of the human arm. Then, when the desired path $\mathcal{P}_{\mathbf{x}_d}$ is to be followed, the kinodynamics of the human arm modify this path, and the end-effector follows the actual path $\mathcal{P}_{\mathbf{x}_{h_G}}$.

Thus, the main idea of this approach is that the actual, modified path $\mathcal{P}_{\mathbf{x}_{h_G}}$ can be used to estimate the parameters of an identification model (Υ). These parameters are the lengths of the human forearm and upper arm ($\mathbf{l}_h \in \mathbb{R}^2$) and the reference frame of the shoulder ($\boldsymbol{\Sigma}_{h_S}$) with respect to the grasping point in the sagittal plane reference frame ($\boldsymbol{\Sigma}_{\mathcal{S}}$), given by

$$\left[\tilde{\mathbf{l}}_h, \tilde{\boldsymbol{\Sigma}}_{h_S}\right] = \Upsilon\left(\mathcal{P}_{\mathbf{x}_{h_G}}\right). \tag{1}$$

Here, the symbol ($\tilde{}$) refers to the estimated parameters. This model is explained in detail in Section III-C.

B. HUMAN ARM DYNAMICS

In pHRI applications, the analysis of interaction wrenches is crucial for developing a safety system [38]. Such an analysis is even more critical in complex human-limb manipulation applications. In this section, the human arm's dynamic model is described, and the wrenches involved in the interaction between the arm and the robot during the estimation movement are analyzed. According to [39], the human arm can be modeled as a 7-degrees of freedom (DoFs) manipulator. When manipulating the arm, the robotic manipulator's acceleration and velocity are low due to safety requirements. Hence, under this assumption, the inertial and Coriolis effects that the robot motion produces on the human arm joint space are reduced. Therefore, the dominant dynamic effects are gravitational. No additional kinematic information about the human arm is acquired when performing motions outside of plane $\mathcal{S}$. Hence, in this study, the task space is limited to the plane $\mathcal{S}$. This constraint is one of the main limitations of the proposed method and is discussed in more detail in Section V.

An impedance Cartesian controller can restrict the task space of the human arm to the plane $\mathcal{S}$ if the axis's impedance perpendicular to the plane and the respective rotational

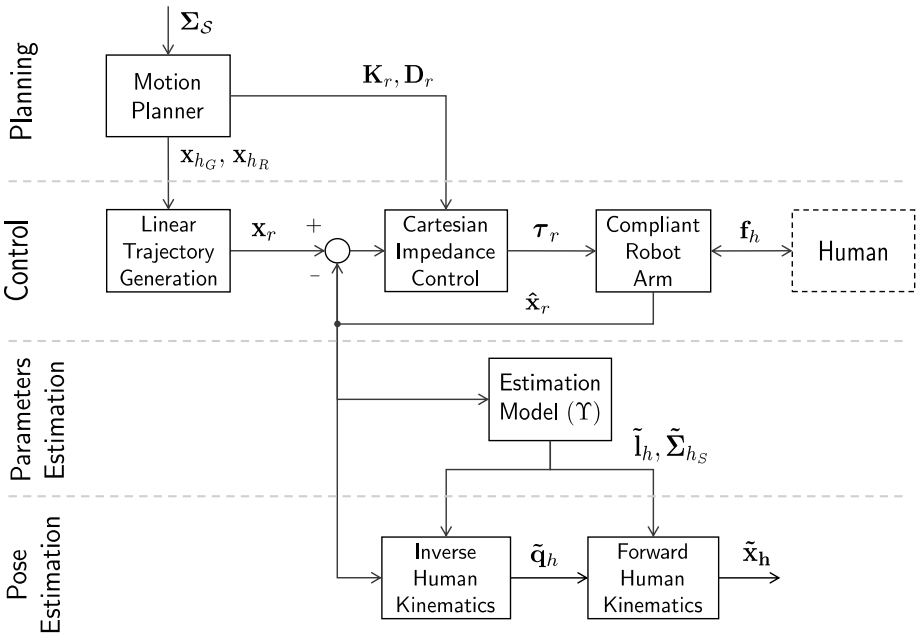

FIGURE 2. Schematic of the proposed approach, divided into four stages: i) planning; ii) control; iii) parameter estimation; iv) pose estimation.

impedance indexes are sufficiently high (see Section III-B). Hence, the following simplification can be considered: The human arm's dynamic behavior, which establishes the dynamic relationships between the human-arm task and joint spaces, can be modeled as a simplified 2-DoF manipulator contained in the sagittal plane, as shown below.

$$\underbrace{\mathbf{M}_h\left(\mathbf{q}_h\right)\ddot{\mathbf{q}}_h}_{\ll \mathbf{g}_h(\mathbf{q}_h)} + \underbrace{\mathbf{C}_h\left(\mathbf{q}_h, \dot{\mathbf{q}}_h\right)\mathbf{q}_h}_{\ll \mathbf{g}_h(\mathbf{q}_h)} + \mathbf{g}_h\left(\mathbf{q}_h\right) = \underbrace{\boldsymbol{\tau}_h}_{0} + \mathbf{J}_h^T\left(\mathbf{q}_h\right)\mathbf{f}_h, \tag{2}$$

where $\mathbf{q}_h \in \mathbb{R}^2$ defines the joint space configuration, $\mathbf{M}_h \in \mathbb{R}^{2\times 2}$ is the symmetric and positive mass matrix, $\mathbf{C}_h \in \mathbb{R}^{2\times 2}$ is the Coriolis matrix, $\mathbf{g}_h \in \mathbb{R}^2$ and $\boldsymbol{\tau}_h \in \mathbb{R}^2$ are the gravity and torque vectors, respectively, $\mathbf{J}_h^T \in \mathbb{R}^{2\times 2}$ is the Jacobian matrix, and $\mathbf{f}_h \in \mathbb{R}^3$ is the interaction force vector of the human arm.

As defined by (2), the most significant dynamic effects on the human arm during the estimation motion are gravitational; thus, no damage is caused to the human arm joints due to the applied wrenches. Similarly, the impedance-based controller, which defines the dynamic robotic behavior, ensures that the human-arm joint space limits are not violated. Details regarding the motion planning and Cartesian impedance controller are provided in Sections III-A and III-B, respectively.

III. LIMB ESTIMATION METHOD

This section describes the four structural elements of the architecture shown in Fig. 2: i) planning, ii) control, iii) parameter estimation, and iv) pose estimation.

A. MOTION PLANNING

At the beginning of the operation, the robot's end-effector is located at $\mathbf{x}_{h_G}$. This point can be previously set by an operator or can be autonomously calculated by the robot using computer vision techniques, such as the one presented in [40]. However, the performance of these methods is sensitive to lighting conditions. Besides, possible occlusions caused by clothes or bed sheets may render these methods ineffective. Nevertheless, the method to obtain $\mathbf{x}_{h_G}$ is beyond the scope of this work. The proposed approach is based on common robotic rehabilitation procedures [41], in which the gripper is manually placed by a human supervisor (therapist). Once the gripper grasps the arm, the center of the grasp and its orientation are recorded, and thus, $\boldsymbol{\Sigma}_\mathcal{S}$ is set. Similarly, the sagittal plane, which is the vertical plane that contains the gripper XZ-axis, is also obtained. For convenience, the XZ-coordinates are taken as the coordinates of $\mathcal{S}$ (see Section IV-B).

To identify the kinematic parameters, the manipulator must perform the following operation (see Fig. 1): at the beginning of the operation, the human arm is placed on a flat surface (e.g., a bed or a table), and the gripper grasps the wrist at $\mathbf{x}_{h_G}$. Then, a trajectory command to move the arm from $\mathbf{x}_{h_G}$ to a point ($\mathbf{x}_{h_R} \in \mathbb{R}^3$) is transmitted to the robot. This point is pre-computed from $\mathbf{x}_{h_G}$, considering an initial joint positions of the human arm with $q_{h_0} = 0$, final joint positions $q_{h_f} = \pi/4$, and lengths $l_{h_0} = 300\,mm$. Then, $\mathbf{x}_{h_R}$ is computed as follows:

$$\mathbf{x}_{h_R} = \begin{bmatrix} x_{h_G} + l_{h_0}\left(\cos\left(q_{h_f}\right) + 1\right) \\ z_{h_G} + l_{h_0}\left(\sin\left(q_{h_f}\right) + 1\right) \\ \psi_{h_G} + \frac{\pi}{2} \end{bmatrix}. \tag{3}$$

The robot tries to follow a linear interpolation path ($\mathcal{P}_{\mathbf{x}_d}$) between $\mathbf{x}_{h_G}$ and $\mathbf{x}_{h_R}$ (see Fig. 1). The actual path ($\mathcal{P}_{\mathbf{x}_{h_G}}$) depends on the human arm parameters, such as the link weights and lengths. $\mathbf{x}_{h_G}$ is used to identify the kinematic parameters using two estimation methods: the generalized Hough transform (HT) [42] and the least squares method (LS) (see Section III-C).

B. ROBOT CONTROL

The estimation must be conducted under an impedance control scheme to ensure that the robot follows a path within the natural human arm range of motion. This section describes the employed impedance controller. We consider the dynamic model of a generic n-DoF manipulator, which is defined as follows:

$$\mathbf{M}_r\left(\mathbf{q}_r\right)\ddot{\mathbf{q}}_r + \mathbf{C}_r\left(\mathbf{q}_r, \dot{\mathbf{q}}_r\right)\dot{\mathbf{q}}_r + \mathbf{g}_r\left(\mathbf{q}_r\right) = \boldsymbol{\tau}_r + \boldsymbol{\tau}_{r_{ext}}, \quad (4)$$

where the subindex r refers to the robotic manipulator, $\mathbf{q}_r \in \mathbb{R}^n$ defines the joint space configuration, $\mathbf{M}_r\left(\mathbf{q}_r\right) \in \mathbb{R}^{n\times n}$ is the symmetric and positive mass matrix, $\mathbf{C}_r\left(\mathbf{q}_r, \dot{\mathbf{q}}_r\right) \in \mathbb{R}^{n\times n}$ is the Coriolis matrix, $\mathbf{g}_r\left(\mathbf{q}_r\right) \in \mathbb{R}^n$ and $\boldsymbol{\tau}_r \in \mathbb{R}^n$ are the gravity and input torque vectors, respectively, and $\boldsymbol{\tau}_{r_{ext}} \in \mathbb{R}^n$ is the external torque vector.

Although the proposed estimation methodology is valid for both redundant and non-redundant manipulators, the former type with seven DoFs ($n = 7$) was used in this study, and the impedance controller described below is of this type as well. Impedance controllers for non-redundant manipulators are described in [43]. To design a Cartesian impedance controller for a redundant manipulator, an end-effector dynamic model in the operational space [44] is required:

$$\boldsymbol{\Lambda}_r\left(\mathbf{q}_r\right)\ddot{\mathbf{x}}_r + \boldsymbol{\mu}_r\left(\mathbf{q}_r, \dot{\mathbf{q}}_r\right)\dot{\mathbf{x}}_r + \mathbf{f}_{r_g}\left(\mathbf{q}_r\right) = \mathbf{f}_r + \mathbf{f}_{r_{ext}}, \quad (5)$$

where $\mathbf{x}_r \in \mathbb{R}^6$ is the task coordinate vector in Cartesian space, $\boldsymbol{\Lambda}_r(\mathbf{q}_r) \in \mathbb{R}^{6\times6}$ is the end-effector inertia matrix, $\boldsymbol{\mu}_r(\mathbf{q}_r, \dot{\mathbf{q}}_r) \in \mathbb{R}^{6\times6}$ is the Cartesian Coriolis matrix, and $\mathbf{f}_{r_g}\left(\mathbf{q}_r\right) = \mathbf{J}_r^{\dagger T}\left(\mathbf{q}_r\right)\mathbf{g}_r\left(\mathbf{q}_r\right) \in \mathbb{R}^6$, $\mathbf{f}_r = \mathbf{J}_r^{\dagger T}\left(\mathbf{q}_r\right)\boldsymbol{\tau}_r \in \mathbb{R}^6$, and $\mathbf{f}_{r_{ext}} \in \mathbb{R}^6$ are the gravitational, control, and external forces vectors, respectively. Notably, only the end-effector dynamics are considered in (5); the null-space dynamics are not included. The matrix $\mathbf{J}^{\dagger}\left(\mathbf{q}_r\right)$ is the dynamically consistent generalized inverse of the Jacobian matrix, which is defined as

$$\mathbf{J}_r^{\dagger}\left(\mathbf{q}_r\right) = \mathbf{M}_r^{-1}\left(\mathbf{q}_r\right)\mathbf{J}_r^T\left(\mathbf{q}_r\right)\left(\mathbf{J}_r\left(\mathbf{q}_r\right)\mathbf{M}_r^{-1}\left(\mathbf{q}_r\right)\mathbf{J}_r^T\left(\mathbf{q}_r\right)\right)^{-1}. \quad (6)$$

The end-effector inertia matrix $\boldsymbol{\Lambda}_r(\mathbf{q}_r)$ and the Cartesian Coriolis matrix $\boldsymbol{\mu}_r(\mathbf{q}_r, \dot{\mathbf{q}}_r)$ can be computed as in [45]:

$$\boldsymbol{\Lambda}_r(\mathbf{q}_r) = \left(\mathbf{J}_r\left(\mathbf{q}_r\right)\mathbf{M}_r^{-1}\left(\mathbf{q}_r\right)\mathbf{J}_r^T\left(\mathbf{q}_r\right)\right)^{-1}, \quad (7)$$

$$\boldsymbol{\mu}_r(\mathbf{q}_r, \dot{\mathbf{q}}_r)\dot{\mathbf{x}}_r = \boldsymbol{\Lambda}_r(\mathbf{q}_r)\left(\boldsymbol{J}_r\left(\mathbf{q}_r\right)\mathbf{M}_r^{-1}\left(\mathbf{q}_r\right)\mathbf{C}_r\left(\mathbf{q}_r, \dot{\mathbf{q}}_r\right) - \dot{\mathbf{J}}_r\left(\mathbf{q}_r\right)\right)\dot{\mathbf{q}}_r. \quad (8)$$

During the estimation movement, the desired robot behavior is similar to that of a mass–spring–damper system:

$$\boldsymbol{\Lambda}_d\ddot{\mathbf{x}}_e + \mathbf{D}_r\dot{\mathbf{x}}_e + \mathbf{K}_r\mathbf{x}_e = \mathbf{f}_{r_{ext}}, \quad (9)$$

where $\mathbf{x}_e = \mathbf{x}_r - \mathbf{x}_d$ is the position error between the robot position $\mathbf{x}_r$ and the desired virtual equilibrium position $\mathbf{x}_d$; and $\boldsymbol{\Lambda}_d \in \mathbb{R}^{6\times6}$, $\mathbf{D}_r \in \mathbb{R}^{6\times6}$, and $\mathbf{K}_r \in \mathbb{R}^{6\times6}$ are the desired inertia, damping, and stiffness matrices of the end-effector, respectively. $\boldsymbol{\Lambda}_d$, $\mathbf{K}_r$, and $\mathbf{D}_r$ are constant, symmetric positive-definite matrices.

For simplicity, the desired end-effector inertia matrix is set as identical to the robot end-effector inertia matrix, $\boldsymbol{\Lambda}_d = \boldsymbol{\Lambda}_r\left(\mathbf{q}_r\right)$. In addition, to ensure the passivity and stability of the system with a time-varying inertia matrix, the Coriolis matrix must be included. The stability proof of that argument is developed in detail in [46]. Thus, equation (9) can be rewritten as

$$\boldsymbol{\Lambda}_r\left(\mathbf{q}_r\right)\ddot{\mathbf{x}}_e + \left(\boldsymbol{\mu}_r\left(\mathbf{q}_r, \dot{\mathbf{q}}_r\right) + \mathbf{D}_r\right)\dot{\mathbf{x}}_e + \mathbf{K}_r\mathbf{x}_e = \mathbf{f}_{r_{ext}}. \quad (10)$$

Moreover, as the end-effector inertia matrix depends on the end-effector pose, the damping matrix should not be constant for the same reason as the one mentioned earlier. A robot pose-dependent damping matrix is defined in [47].

Therefore, the desired robot behavior can be achieved by the following control law:

$$\mathbf{f}_{r_{ext}} = \mathbf{f}_{r_g}\left(\mathbf{q}_r\right) + \boldsymbol{\Lambda}_r\left(\mathbf{q}_r\right)\ddot{\mathbf{x}}_d + \boldsymbol{\mu}_r\left(\mathbf{q}_r, \dot{\mathbf{q}}_r\right)\dot{\mathbf{x}}_d - \mathbf{D}_r\left(\mathbf{q}_r\right)\dot{\mathbf{x}}_e - \mathbf{K}_r\mathbf{x}_e. \quad (11)$$

The input torque of the Cartesian impedance controller is then defined as

$$\boldsymbol{\tau}_r = \mathbf{g}\left(\mathbf{q}_r\right) + \mathbf{J}_r^T\left(\mathbf{q}_r\right)\left(\boldsymbol{\Lambda}_r\left(\mathbf{q}_r\right)\ddot{\mathbf{x}}_d + \boldsymbol{\mu}_r\left(\mathbf{q}_r, \dot{\mathbf{q}}_r\right)\dot{\mathbf{x}}_d - \mathbf{D}_r\left(\mathbf{q}_r\right)\dot{\mathbf{x}}_e - \mathbf{K}_r\mathbf{x}_e\right). \quad (12)$$

Thus, by assuming that the interaction wrenches with the human arm are the only ones applied to the manipulator during the estimation, we can state that $\mathbf{f}_{r_{ext}} = \mathbf{f}_h$. In addition, once the robot grasps the arm on $\mathbf{x}_{h_G}$ we can assume that $\hat{\mathbf{x}}_r = \mathbf{x}_{h_G}$ during the entire manipulation process, and this is true only when the grasping is stable. In this study, zero slippage and a stable grasp during the entire manipulation process were considered because this problem is not a part of this work and should be considered separately.

C. PARAMETER ESTIMATION

Once the task, the controller, and motion planning are set, multiple methodologies can be used as an estimation model Υ [48]. This works uses and compares the performance of HT and LS approaches.

a: Hough Transform:

HT is a feature extraction technique used in computer vision. It was primarily designed for line detection [49], although it is also capable of identifying any arbitrary curve. It is based on a voting procedure performed in the parametric space ($\mathbb{P}$), through which candidates are obtained as local maxima in the

accumulator space ($\mathbb{A}$). We know that $\mathbf{x}_{h_G}$ and $\mathbf{x}_{h_E}$ describe a circumference with centers in $\mathbf{x}_{h_E}$ and $\mathbf{x}_{h_S}$, respectively. These circumferences ($\mathcal{C}$) are defined by

$$\mathcal{C}\left\{r,s,t\right\} \equiv \left(x_{h_G}-s\right)^2+\left(z_{h_G}-t\right)^2=r^2, \tag{13}$$

where r denotes the radius, and s and t are the coordinates of the center in $\mathcal{S}$, respectively. Then, we define the accumulator matrix ($\mathbf{A} \in \mathbb{N}^{\rho\times\sigma\times\varsigma}$) as

$$\mathbf{A} = \begin{array}{c} \\ s \\ \\ \\ \\ \\ \end{array} \begin{array}{c} \begin{array}{ccccc} {}^{\rho}a_1^1 & {}^{\rho}a_2^1 & {}^{\rho}a_3^1 & \cdots & {}^{\rho}a_{\varsigma}^1 \end{array} \\ \begin{array}{ccccc} \cdots & \cdots & \cdots & \cdots & \cdots \end{array} \\ \begin{array}{ccccc} {}^{2}a_1^1 & {}^{2}a_2^1 & {}^{2}a_3^1 & \cdots & {}^{2}a_{\varsigma}^1 \end{array} \\ \begin{array}{ccccc} {}^{1}a_1^1 & {}^{1}a_2^1 & {}^{1}a_3^1 & \cdots & {}^{1}a_{\varsigma}^1 \end{array} \\ \begin{array}{ccccc} {}^{1}a_1^2 & {}^{1}a_2^2 & {}^{1}a_3^2 & & {}^{1}a_{\varsigma}^2 \end{array} \\ \begin{array}{ccccc} {}^{1}a_1^3 & {}^{1}a_2^3 & {}^{1}a_3^3 & & {}^{1}a_{\varsigma}^3 \end{array} \\ \begin{array}{ccccc} \vdots & & & \ddots & \end{array} \\ \begin{array}{ccccc} {}^{1}a_1^{\sigma} & {}^{1}a_2^{\sigma} & {}^{1}a_3^{\sigma} & & {}^{1}a_{\varsigma}^{\sigma} \end{array} \\ \\ t \end{array} \begin{array}{c} \\ \\ \\ \\ \\ \\ \\ \\ \\ \\ r \end{array}, \tag{14}$$

where ρ, σ, and $\varsigma \in \mathbb{N}$ are the maximum numbers of possible values of r, s, and t, respectively. Each element ${}^{r}a_s^t$ of $\mathbf{A}$ accumulates votes for a certain circumference of the i-th observation.

$${}^{r}a_s^t = \sum_{i=1}^{N} \mathcal{C}\left\{r,s,t\right\}, \tag{15}$$

where N is the total number of observations, defining all possible circumferences in the parameter space ($\mathbb{P} = \{(r,s,t)$, with $s,\, t \in \mathbb{Z},\, r \in \mathbb{N}\}$).

Because each point of the path can fit in infinite circumferences, the following assumptions are made to reduce the search volume and computational load:

1) $\mathcal{S}$ has been discretized with a 1 mm grid:

$$s,\, t \in \mathbb{Z}, \quad r \in \mathbb{N}. \tag{16}$$

2) Considering the common lengths of the parts of the human arm, circumferences with radii greater than $\rho = 500$ mm are disregarded:

$$s \in \left[x_{h_G}-\rho,\, x_{h_G}+\rho\right], \quad \sigma,\varsigma = 2\,\rho. \tag{17}$$

3) The centers of the circumferences are normal to the path of the end-effector:

$$t = z_{h_G} + \left(s - x_{h_G}\right)\, tan(\psi_{h_G}). \tag{18}$$

Based on these considerations, we can define HT algorithm ($\mathcal{H}\left(\mathcal{P}_{\mathbf{x}}\right)$) described in Algorithm 1 for a certain path with N observations $\mathcal{P}_{\mathbf{x}} = \{\mathbf{x}_1, \ldots, \mathbf{x}_i, \ldots, \mathbf{x}_N\}$. This algorithm calculates the most voted curve $\mathcal{C}^*\left\{r^*,s^*,t^*\right\}$ and returns the radius of this curve (r^*), which is used to estimate the distances of the parts of the human arm.

Algorithm 1 $\mathcal{H}\left(\mathcal{P}_{\mathbf{x}}\right)$

```
Initialize A: A = 0
for i = 1 : N do
  for s = x_i − ρ : x_i + ρ do
    Compute t: t(x_i, s) ← (18)
    Compute r: r(x_i, s, t) ← (13)
    if r ≤ ρ then
      Update A(r, s, t): ^r a_s^t = ^r a_s^t + 1
    end if
  end for
end for
Get C*: C*{r*, s*, t*} ← argmax_{r,s,t} A(r, s, t)
return r*
```

Once the radius of the circumference is identified, the pose of its center ($\mathbf{x}_c$) can be computed with respect to a certain point $\mathbf{x}_i$ on the path, according to the function $\mathcal{F}\left(\mathbf{x}_i, r^*\right)$

$$\mathcal{F}\left(\mathbf{x}_i, r^*\right) \equiv \begin{cases} x_c = & x_i - r^* \cdot cos(\psi_i) \\ z_c = & z_i - r^* \cdot sin(\psi_i) \\ \psi_c = & \arctan\left(\frac{\|z_c - z_i\|}{\|x_c - x_i\|}\right) \end{cases} \tag{19}$$

Therefore, the HT identification model can be defined as

$$\Upsilon_{HT}\left(\mathcal{P}_{\mathbf{x}_{h_G}}\right) \equiv \begin{cases} \tilde{l}_{h_2} = & \mathcal{H}\left(\mathcal{P}_{\tilde{\mathbf{x}}_{\mathbf{r}}}\right) \\ \tilde{l}_{h_1} = & \mathcal{H}\left(\mathcal{P}_{\tilde{\mathbf{x}}_{\mathbf{h_E}}}\right) \\ \tilde{\mathbf{\Sigma}}_{h_S} = & \mathcal{F}\left(\tilde{\mathbf{x}}_{h_E}, \tilde{l}_{h_1}\right) \end{cases}, \tag{20}$$

where the estimation of the elbow pose with respect to the grasping point is given by

$$\tilde{\mathbf{x}}_{h_e} = \mathcal{F}\left(\tilde{\mathbf{x}}_{h_G}, \tilde{l}_{h_2}\right). \tag{21}$$

b: Least Squares

On the other hand, LS is a standard approach widely used in regression analysis and parameter estimation [50]–[52]. It is based on the adjustment of the parameters of a model function to best fit a data set by minimizing the sum of the squares of the residuals [53]. Let $\{(v_k, w_k)\}_{k=1}^{n}$ be a data set of n observations composed of a scalar output w_k and a vector input $v_k \in \mathbb{R}^m$ with $n > m$. Hence, the goal is to find a function $f\left(v\right)$ such that $f\left(v_k\right) \approx w_k$:

$$w_k = f\left(v_k\right) = u_1 v_1 + \cdots + u_m v_m. \tag{22}$$

Expanding (22) for the n observations of the data set one obtain an overdetermined linear system which can be written in matrix form as

$$\mathbf{V}\boldsymbol{u} = \mathbf{W}, \tag{23}$$

where $\mathbf{V}$ is the coefficient matrix, $\boldsymbol{u}$ is the vector of unknowns, and $\mathbf{W}$ is the constant terms matrix. According to [54], the vector of unknowns $\boldsymbol{u}$ that minimizes the quadratic error is given by

$$\hat{\boldsymbol{u}} = \left(\mathbf{V}^T\mathbf{V}\right)^{-1}\mathbf{V}^T\mathbf{W} \tag{24}$$

As mentioned above, $\mathbf{x}_{h_G}$ and $\mathbf{x}_{h_E}$ describe a circumference. To estimate the parameter of such a circumference with least squares method, one should express (13) in a more appropriate form:

$$u_1 x_{h_G} + u_2 z_{h_G} - u_3 = x_{h_G}^2 + z_{h_G}^2, \tag{25}$$

where $u_1 = 2s$, $u_2 = 2t$ and $u_3 = \left(s^2 + t^2 - r^2\right)$. Evaluating (25) for the whole set of points of the path yields an overdetermined system of N linear equations and 3 unknowns as the one shown in (23). Then, one can define the vector of unknowns $\boldsymbol{u} = [u_1, u_2, u_3]^T$, the coefficient matrix $\mathbf{V}$ and the constant terms matrix $\mathbf{W}$ as:

$$\begin{aligned} \mathbf{V} &= \begin{bmatrix} x_{h_{G1}} & z_{h_{G1}} & -1 \\ \vdots & \vdots & \vdots \\ x_{h_{GN}} & z_{h_{GN}} & -1 \end{bmatrix}, \\ \mathbf{W} &= \begin{bmatrix} x_{h_{G1}}^2 + z_{h_{G1}}^2 \\ \vdots \\ x_{h_{GN}}^2 + z_{h_{GN}}^2 \end{bmatrix}. \end{aligned} \tag{26}$$

Thus, obtaining $\boldsymbol{u}$ as in (24), the radius of the circumference that offers the best fit to the path is given by

$$r = \mathcal{LS}\left(\mathcal{P}_{\mathbf{x}}\right) = \sqrt{\left(\frac{u_1}{2}\right)^2 + \left(\frac{u_2}{2}\right)^2 - u_3}. \tag{27}$$

Once the radius is estimated, the pose of its center can be obtained by (19). Hence, the LS identification model if finally defined as

$$\Upsilon_{LS}\left(\mathcal{P}_{\mathbf{x}_{h_G}}\right) \equiv \begin{cases} \tilde{l}_{h_2} = & \mathcal{LS}\left(\mathcal{P}_{\tilde{\mathbf{x}}_{\mathbf{r}}}\right) \\ \tilde{l}_{h_1} = & \mathcal{LS}\left(\mathcal{P}_{\tilde{\mathbf{x}}_{\mathbf{h_E}}}\right) \\ \tilde{\boldsymbol{\Sigma}}_{h_S} = & \mathcal{F}\left(\tilde{\mathbf{x}}_{h_E}, \tilde{l}_{h_1}\right) \end{cases}, \tag{28}$$

where the estimation of the elbow pose is obtained by (21).

D. LIMB POSE ESTIMATION FOR SAFE MANIPULATION

Once the kinematic model parameters have been estimated, one can obtain the Cartesian and joint coordinates of the human arm. These are crucial in order to ensure safe planning of human limb movement in two ways:

1) Restrict the human joints inside the safe range, which may differ depending on the subject. This requirement is fulfilled by the inverse kinematic model of the human upper limb.
2) Prevent collisions of the human arm with the environment, which is also important for a safe planning of the placement motion.

Inverse and forward kinematic models of the human arm in $\mathcal{S}$ can be easily obtained using a geometric approach and are defined by (29) and (30), respectively.

$$\mathbf{q}_h = \begin{bmatrix} \arctan\left(\frac{x_{h_G} - l_{h_2}\cos\left(\psi_{h_G}\right)}{y_{h_G} - l_{h_2}\sin\left(\psi_{h_G}\right)}\right) \\ \psi_{h_G} - \arctan\left(\frac{x_{h_G} - l_{h_2}\cos\left(\psi_{h_G}\right)}{y_{h_G} - l_{h_2}\sin\left(\psi_{h_G}\right)}\right) \end{bmatrix}, \tag{29}$$

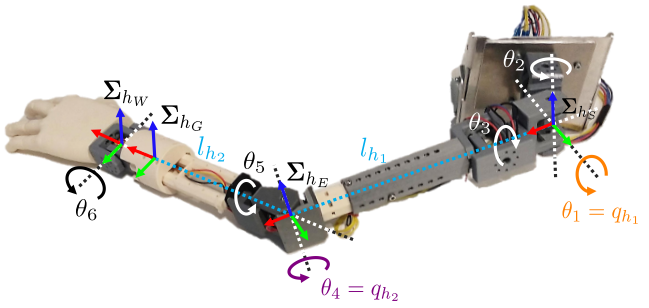

FIGURE 3. A 6-DoF 3D-printed, customizable, and sensorized anthropomorphic arm that simulates the human arm's kinodynamic behavior is used as a dummy for experimental validation of the proposed methodology.

where x_{h_G}, y_{h_G}, ψ_{h_G} are the elements of $\mathbf{x}_{h_G}$.

$$\begin{aligned} \mathbf{x}_{h_E} &= \begin{bmatrix} l_{h_1}\cos\left(q_{h_1}\right) \\ l_{h_1}\sin\left(q_{h_1}\right) \\ q_{h_1} \end{bmatrix} + \boldsymbol{\Sigma}_{h_S}, \\ \mathbf{x}_{h_G} &= \begin{bmatrix} l_{h_2}\cos\left(q_{h_1} + q_{h_2}\right) \\ l_{h_2}\sin\left(q_{h_1} + q_{h_2}\right) \\ q_{h_1} + q_{h_2} \end{bmatrix} + \mathbf{x}_{h_E}, \end{aligned} \tag{30}$$

where l_{h_1} and l_{h_2} are the elements of $\mathbf{l}_h$; q_{h_1} and q_{h_2} are the elements of $\mathbf{q}_h$; and $\mathbf{x}_{h_G}$ and $\mathbf{x}_{h_E}$ are calculated with respect to the reference frame at the shoulder of the human arm $\boldsymbol{\Sigma}_{h_S}$.

IV. EXPERIMENTS

To evaluate the performance of the proposed approach, the ground-truth data, including the actual kinematic parameters of the limbs and the joint value trajectories, must be obtained. For this purpose, a sensorized dummy with configurable lengths and weights is used (see Fig. 3).

A. DUMMY ARM

The core design of the dummy is similar to that of the bones of a human arm. Conceptually, the dummy can be 3D-printed using common FDM 3D-printers. It has six DoFs: a three-joint spherical shoulder, a two-joint elbow, and a simplified single-joint wrist. Note that the dummy has 6-DoFs whereas a human upper-limb has 7-DoFs. The missing dummy DoF corresponds to the wrist abduction/adduction. Since the robot graps the forearm, wrist DoFs do not affect the estimation movement. The dummy's kinematic behavior mimics that of a real human arm, including the joint range of motion. This device is modular as it allows for modifications in the link lengths. Therefore, to alter the length of the humerus (l_{h1}), links of different lengths can be used. A cylindrical ring of diameter $60mm$ serves as the forearm grasping point, imitating the shape of a human wrist. This ring can be placed at different locations along the "ulna-radius" segment, allowing for modifications in the length l_{h2}. To imitate the dynamic behavior of a human arm, additional weights are

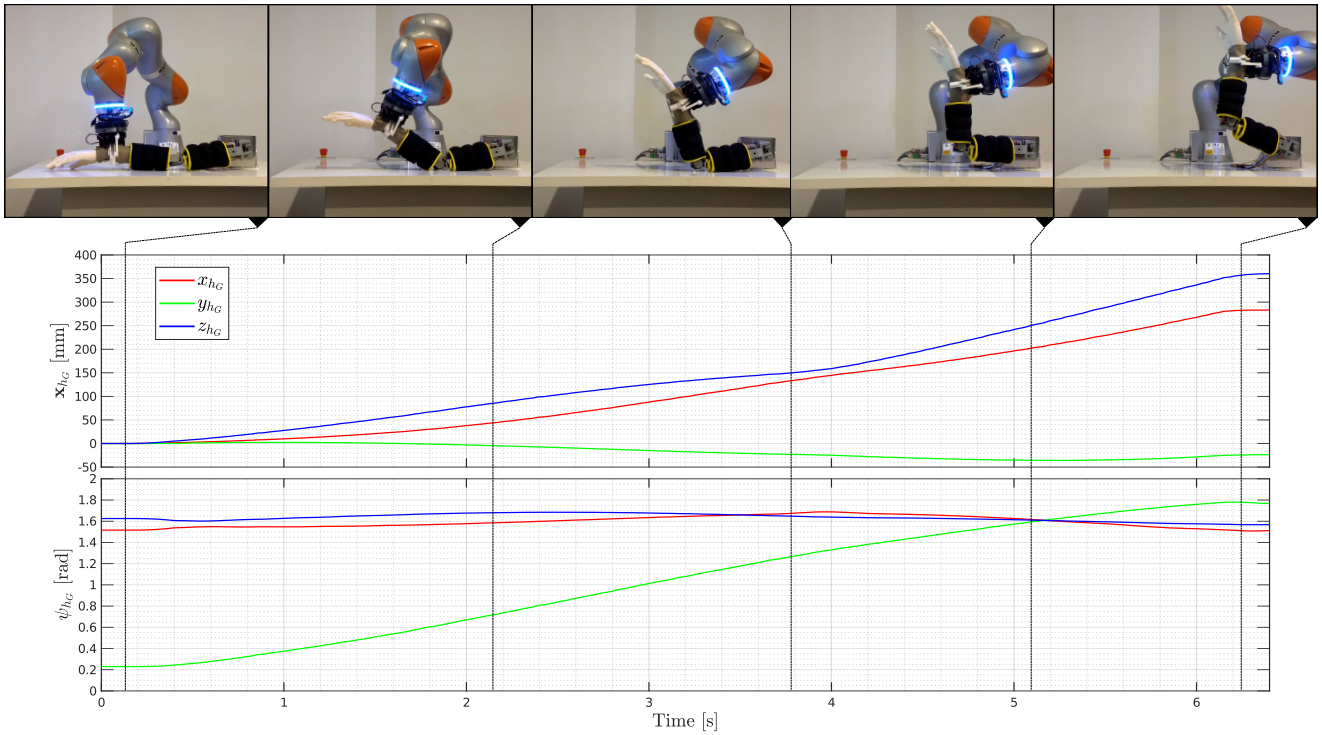

FIGURE 4. Time-lapse of one of the experiments (top), positions (top graph) and orientations (bottom graph) of $\mathbf{x}_{h_G}$ during the execution of one experiment. Although the position deviates a little from $\mathcal{S}$, the predominant motion occurs in $\mathcal{S}$. The same effect can be observed in the orientation, where the most significant change occurs in the axis perpendicular to $\mathcal{S}$ (Y-axis).

attached around the artificial bones. The complete system design is available for download from a public repository [1].

Analog linear potentiometers built into the six DoFs measure the joint coordinates of the arm, θ_h. An Arduino Mega2560 microcontroller maps the electrical signals to angular values, with a 100 Hz sampling rate. The microcontroller integrates a 10-bit ADC. Hence, the joint angles are measured with a resolution of 0.0047 rad. Because the movements in $\mathcal{S}$ are the only ones considered in this study, only two joints of the arm are observed (see Fig. 3).

B. EXPERIMENT DESIGN

A KUKA iiwa lbr 7R robot is used for the experiments. The impedance controller can be programmed with specific Cartesian stiffness $\mathbf{K}_r$ and damping $\mathbf{D}_r(q)$ matrices. $\mathbf{K}_r$ was implemented as a diagonal matrix whose values were chosen to enable a lifting motion of the human arm in $\mathcal{S}$ and simultaneously restrict motion in other directions.

For safety reasons, $\mathbf{D}_r(q,)$ is tuned in order to provide an overdamped behavior. Under such compliant control, the resulting trajectory and forces exerted by the end-effector depend on the interaction wrenches applied by the subject, which, during lifting, is assumed to be passive (i.e., $\tau_h = 0$). Nevertheless, the next additional safety measures are included in the robot controller to ensure safe manipulation even when the subject plays an active role in the task: the velocity of the robot is limited to 2.5% of the maximum reachable speed to minimize the risk of injury; moreover, the maximum force that the robot could exert and the Cartesian workspace are constrained. Thus, the robot cannot exceed the natural range of motion of the human joints.

Six experiments are performed using the same link weights ($\mathrm{m}_1 = 1.55$ kg, $\mathrm{m}_2 = 1.317$ kg) but with variable lengths. With the dummy shoulder fixed to the table, the robot is guided manually to $\mathbf{x}_{h_G}$. Once the wrist is grasped, the manipulator follows the trajectory specified in Section III-A. As the grasping point is the only known point, all computations and measurements are performed with reference to this point. During the experiments, end-effector Cartesian poses and dummy joints positions data are collected. All measurements are recorded at a sampling rate of 100 Hz. For simplicity, the plane $\mathcal{S}$ and the XZ plane of the robot reference framework are defined as parallel.

V. RESULTS AND DISCUSSION

In Fig. 4 the estimation trajectory performed by the robot is shown. The sequence of images at the top illustrate the experiment process, which have been recorded in video [2]. The Cartesian trajectory in position (graph at the top) and orientation (graph at the bottom) of $\mathbf{x}_{h_G}$ is shown. As can be seen, the motion does not constraint perfectly to the $\mathcal{S}$-plane; there exist a little divergence from that plane. Nevertheless,

[1] www.github.com/Taislab/dummyarm

[2] https://youtu.be/cNCqYyKOUVM

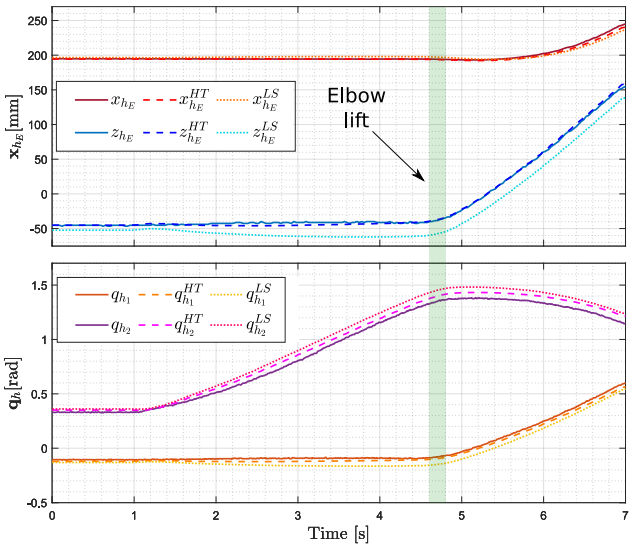

FIGURE 5. Ground-truth and estimated Cartesian trajectories (top) and joint trajectories (bottom) for the elbow in one experiment. The green region indicates the time at which the elbow starts to lift.

the main component of the motion is contained in $\mathcal{S}$, so the simplifications of the model of the human arm made in Section II-B are valid.

The performance of the proposed methodology is evaluated by comparing the ground truth and estimated trajectories. The outcomes are shown in Fig. 5, where the top plot represents the Cartesian trajectories of the elbow. The estimated X and Z coordinates are represented by dashed and dotted lines for estimations performed by HT and LS, respectively, whereas the ground truth data are denoted by continuous lines. The plot at the bottom presents the trajectories of the two joints of the dummy arm.

Fig. 6 presents plots of the Cartesian paths in $\mathcal{S}$ for the six experiments. These graphs show that the HT-estimated, the LS-estimated and the ground-truth elbow positions, marked with circles, asterisks and crosses, respectively, follow similar trajectories. The predicted shoulder position, marked with a triangle and a diamond for HT and LS, respectively, presents a more significant estimation error. This is due to the estimation process: as described in Section III-C, the proposed method first estimates the pose of the elbow, $\tilde{\mathbf{x}}_{h_E}$; then, $\tilde{\mathbf{x}}_{h_E}$ is used to estimate the pose of the shoulder, $\tilde{\mathbf{x}}_{h_S}$. Thus, $\tilde{\mathbf{x}}_{h_S}$ includes the accumulated errors of both the elbow and shoulder estimations.

Table 1 presents a summary of the results, including the actual and estimated link lengths for each experiment, and the estimation errors. Between the length estimations ($\tilde{l}_{h_1}$ and $\tilde{l}_{h_2}$), the former exhibits a lower error than the latter owing to the aforementioned accumulation error. The same effect is observed for shoulder estimation, which is performed from $\tilde{l}_{h1}$. The joint and Cartesian estimation errors are represented by the mean value and the standard deviation of the root-mean-square-error (RMSE) function. The error accumulation effects are more prominent in the elbow and shoulder pose estimations. As expected, the elbow positions exhibit lower errors than the shoulder positions. Compared with LS, HT can handle non-locality better and is more robust to noise, as noisy points are unlikely to contribute to a single cell. In terms of computational complexity, the time needed for the estimation varies with the number of points recorded during the motion. For a path of 300 points, HT takes $1,7334$ seconds whereas LS takes $0,0051$ seconds, using in an Intel Core i7-3630 computer with 8GB of RAM. Considering the functioning of each method (Section III-C), it is obvious that HT is more complex than LS, but the difference in time is also explained in terms of implementation. For the implementation of LS, we used the *MatLab Curve Fitting Toolbox*, which provides highly optimized algorithms for regression and parameter estimation. On the other hand, HT has been implemented from scratch. The implementation of HT is not complicated as only three parameters are considered, but the code generated has not been optimized. Even though HT takes almost 2 seconds to complete the estimation, it is fast enough to not interfere with a possible rehabilitation task. The results confirm the initial hypothesis: HT is a highly suitable method to identify any circumference present in the path, such as that followed by the wrist during the identification of the trajectory. Despite the accumulated error, the estimated pose of the upper arm is highly accurate, with errors lower than 1 cm.

Based on the results, it can be concluded that the proposed method functioned appropriately. The method is capable of estimating the kinematic model of human upper limbs without the use of external sensors. Therefore, the results demonstrate that the proposed methodology can be used as a preparatory step in rehabilitation and assistive applications in which the human arm kinematic model needs to be accurately defined. Nevertheless, a few assumptions were incorporated in this study, which limits the applicability of the proposed method to specific real-world tasks.

As previously discussed, robotic manipulation of human limbs is exceptionally complicated and represents a significant challenge in robotics. Multiple aspects related to robotic control, manipulation, artificial intelligence, and physical interaction are yet to be considered; hence, although the proposed methodology offers high accuracy, it involves certain limitations in real-world applications. The first assumption is that the subject's arm is lying down and that the available motions are limited to the sagittal plane. However, although our experiments were conducted under this assumption, the proposed method can be extended to different human postures in the sagittal plane. The subject can also stand or sit as long as the arm and the estimation motion remain in the sagittal plane, with the elbow initially lying on a surface. Nevertheless, for incorporating these postures, the motion planner should be modified, and a new identification path must be defined to fit new human postures.

Second, the subject is considered passive during the parameter estimation. This condition must be fulfilled for cor-

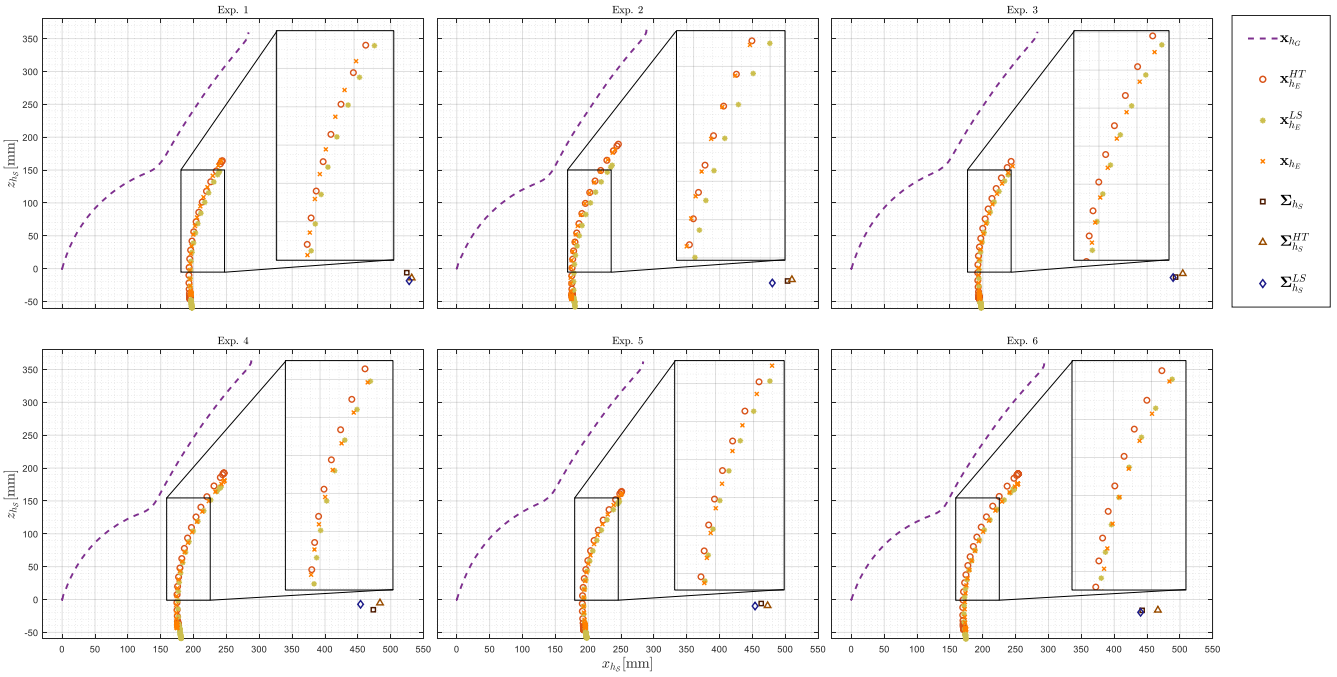

FIGURE 6. Graphical representation of the results obtained for the six experiments in the plane $\mathcal{S}$. For each point of the Cartesian path (purple dotted line) the proposed method estimates the position of the elbow and shoulder of the dummy arm. The circles and the squares represent the actual position of the dummy's elbow and shoulder, respectively. The crosses and the triangles represent the estimated elbow and shoulder poses by HT, while the asterisks and the diamonds represent the estimated elbow and shoulder by LS, respectively. The squared area represent a zoom on the elbow paths to illustrate the differences between the real one, and the ones estimated by HT and LS.

rect functioning of the method. If the subject resists the robot, the considerations discussed in Section II will not be fulfilled. Consequently, the trajectory during the estimation phase may present an erratic shape, and the method may fail. Because of the passive-subject assumption, the human shoulder is considered stationary, that is, it occupies a fixed position in space. This is true when the robot manipulates the human limb under the action of a proper planner. Finally, the method is restricted to the sagittal plane, $\mathcal{S}$. This is the most significant limitation of the method and must be overcome.

The main safety risks involved in robotic manipulation of human limbs include exceeding the joint limits, causing pain or injuries, and collisions with the environment or other body parts. The use of low velocity profiles and impedance control can help minimize range violations or incidences of hitting a surface with the elbow. However, safety cannot be ensured without proper planning. Motion planning can be performed whenever a model of the human arm is available. Methods for collision-free planning and task-space boundaries used in robotics can be applied.

VI. CONCLUSIONS

This paper presented a method for estimating human arm parameters via robotic manipulation. The estimation method utilizes the kinesthetic information of the robot, which moves along a compliant trajectory that can be easily modified based on human arm kinodynamics. The lengths of the links, the joints, and the Cartesian positions of the human arm model were obtained by applying the Hough transform to measurements from the robot position sensors. To evaluate the accuracy of the method, six experiments with different arm lengths were conducted by utilizing a sensorized dummy that provided ground truth measurements. The experimental results demonstrate the effectiveness of the proposed methodology in terms of human arm pose estimation and thus, in terms of safe manipulation.

However, safe manipulation requires specific considerations and depends on the desired task. Hence, the implementation of safe manipulation levels will be further studied for different potential applications, such as elderly care and rehabilitation. In addition, additional safety parameters, such as joint ranges and maximum joint velocities and torques, must be considered in motion planning after the estimation.

Moreover, the absence of calibration processes makes the proposed method a ready-to-use solution, even for non-specialized personnel. The method only requires manually placing the robot at the grasping point and executing the estimation program. In addition, the method offers a generality unseen in the majority of rehabilitation systems. In contrast with existing exoskeletons, our system can be used for any patient without any customization.

In conclusion, the use of a commercial robot manipulator and the presence of only minor errors in the estimation process make the proposed method an excellent alternative to vision-based estimation systems. Although the proposed method involves certain limitations (constraints of the sagittal

TABLE 1. Summary of the results: Ground truth and estimated lengths and mean (μ) and standard deviation (σ) of the RMSE of joints and Cartesian positions. For each experiment, the results obtained with HT and LS are presented at the top and bottom of each cell, respectively, for easy comparison. *Note: The Cartesian position of the shoulder was estimated only once; hence, the standard deviation is 0.

Exp.	l_{h1}	l_{h2}	l_{h1}^{HT} l_{h1}^{LS}	l_{h2}^{HT} l_{h2}^{LS}	$\mu_{q_{h_1}}^{HT}$ $\mu_{q_{h_1}}^{LS}$	$\sigma_{q_{h_1}}^{HT}$ $\sigma_{q_{h_1}}^{LS}$	$\mu_{q_{h_2}}^{HT}$ $\mu_{q_{h_2}}^{LS}$	$\sigma_{q_{h_2}}^{HT}$ $\sigma_{q_{h_2}}^{LS}$	$\mu_{\Sigma_{h_E}}^{HT}$ $\mu_{\Sigma_{h_E}}^{LS}$	$\sigma_{\Sigma_{h_E}}^{HT}$ $\sigma_{\Sigma_{h_E}}^{LS}$	$\mu_{\Sigma_{h_S}}^{HT}$ $\mu_{\Sigma_{h_S}}^{LS}$	$\sigma_{\Sigma_{h_S}}^{HT*}$ $\sigma_{\Sigma_{h_S}}^{LS*}$
1	330	200	339 333.25	199 216.12	$1.3402e^{-2}$ $1.6798e^{-02}$	$6.0851e^{-3}$ $5.8873e^{-3}$	$1.9497e^{-2}$ $4.4404e^{-2}$	$9.3472e^{-3}$ $2.1118e^{-2}$	4.0753 16.387	2.3270 4.0623	11.264 13.021	0 0
2	330	180	335 302.45	179 212.99	$5.9380e^{-3}$ $6.5370e^{-2}$	$4.0687e^{-3}$ $2.9497e^{-2}$	$1.9825e^{-2}$ $5.8048e^{-2}$	$1.6693e^{-2}$ $2.9705e^{-2}$	3.3758 25.450	1.7417 8.9402	7.1496 23.070	0 0
3	300	200	312 295.57	199 219.78	$1.8420e^{-2}$ $5.1236e^{-2}$	$7.0118e^{-3}$ $1.8237e^{-2}$	$3.4763e^{-2}$ $6.7021e^{-2}$	$1.6734e^{-2}$ $2.9390e^{-2}$	2.5047 15.207	1.6050 5.5080	12.994 3.2653	0 0
4	300	180	309 277.93	178 199.79	$2.2668e^{-2}$ $6.7885e^{-2}$	$6.7438e^{-3}$ $2.9639e^{-2}$	$2.3956e^{-2}$ $5.8383e^{-2}$	$1.5699e^{-2}$ $3.0305e^{-2}$	6.3777 12.849	3.3123 4.8660	15.494 21.452	0 0
5	270	200	282 260.77	200 215.91	$8.4200e^{-3}$ $4.3893e^{-2}$	$5.6806e^{-3}$ $1.8253e^{-2}$	$2.7097e^{-2}$ $6.8209e^{-2}$	$1.9907e^{-2}$ $2.3381e^{-2}$	4.3389 15.292	1.3903 4.9043	10.553 9.7634	0 0
6	270	180	297 268.91	174 198.33	$1.7938e^{-2}$ $3.2628e^{-2}$	$7.2856e^{-3}$ $1.7046e^{-2}$	$3.0464e^{-2}$ $7.0260e^{-2}$	$2.3413e^{-2}$ $2.6840e^{-2}$	10.531 10.091	5.2771 4.2329	24.511 2.1565	0 0

plane and offline parameter estimation), it highlights the importance of kinesthetic information. In addition, once the kinematic parameters are estimated, they can be used not only for online tasks but also to detect undesirable behaviors during human arm manipulation. The main advantages of this method are its plug-and-play orientation, improved accuracy compared with that of vision-based methods, and reduced cost and complexity compared with those of non-commercial, bulky exoskeleton-based systems.

Furthermore, this work opens the door to future research in the unexplored field of robotic manipulation of human limbs. Future studies could consider implementing an extended version of the proposed methodology to work beyond the sagittal plane. This approach could also be applied to estimate the dynamics of the human arm during pHRI tasks. In addition, the proposed method will be considered for practical applications with real humans. In this regard, a generalization of the proposed method is desired to be used with humans of different complexion.

REFERENCES

[1] D. Feil-Seifer and M. J. Mataric, "Defining socially assistive robotics," in *International Conference on Rehabilitation Robotics (ICORR)*, 2005, pp. 465–468.

[2] T. Bhattacharjee, G. Lee, H. Song, and S. S. Srinivasa, "Towards robotic feeding: Role of haptics in fork-based food manipulation," *IEEE Robotics and Automation Letters*, vol. 4, no. 2, pp. 1485–1492, 2019.

[3] Z. Erickson, M. Collier, A. Kapusta, and C. C. Kemp, "Tracking human pose during robot-assisted dressing using single-axis capacitive proximity sensing," *IEEE Robotics and Automation Letters*, vol. 3, no. 3, pp. 2245–2252, 2018.

[4] I. Carrera, H. A. Moreno, R. Saltarén, C. Pérez, L. Puglisi, and C. Garcia, "Road: domestic assistant and rehabilitation robot," *Medical & Biological Engineering & Computing*, vol. 49, no. 10, p. 1201, 2011.

[5] J. M. Gandarias, F. Pastor, A. J. Muñoz-Ramírez, A. J. García-Cerezo, and J. M. Gómez-de-Gabriel, "Underactuated gripper with forearm roll estimation for human limbs manipulation in rescue robotics," in *2019 IEEE/RSJ International Conference on Intelligent Robots and Systems (IROS)*, 2019, pp. 5937–5942.

[6] L. Peternel, W. Kim, J. Babič, and A. Ajoudani, "Towards ergonomic control of human-robot co-manipulation and handover," in *IEEEh International Conference on Humanoid Robotics (Humanoids)*, 2017, pp. 55–60.

[7] A. J. Westerveld, B. J. Aalderink, W. Hagedoorn, M. Buijze, A. C. Schouten, and H. v. d. Kooij, "A damper driven robotic end-point manipulator for functional rehabilitation exercises after stroke," *IEEE Transactions on Biomedical Engineering*, vol. 61, no. 10, pp. 2646–2654, 2014.

[8] A. Basteris, S. M. Nijenhuis, A. H. Stienen, J. H. Buurke, G. B. Prange, and F. Amirabdollahian, "Training modalities in robot-mediated upper limb rehabilitation in stroke: a framework for classification based on a systematic review," *Journal of NeuroEngineering and Rehabilitation*, vol. 11, no. 1, p. 111, 2014.

[9] B. R. Brewer, S. K. McDowell, and L. C. Worthen-Chaudhari, "Poststroke upper extremity rehabilitation: A review of robotic systems and clinical results," *Topics in Stroke Rehabilitation*, vol. 14, no. 6, pp. 22–44, 2007.

[10] G. Sprint, D. J. Cook, D. L. Weeks, and V. Borisov, "Predicting functional independence measure scores during rehabilitation with wearable inertial sensors," *IEEE Access*, vol. 3, pp. 1350–1366, 2015.

[11] A. Pennycott, D. Wyss, H. Vallery, V. Klamroth-Marganska, and R. Riener, "Towards more effective robotic gait training for stroke rehabilitation: a review," *Journal of NeuroEngineering and Rehabilitation*, vol. 9, no. 1, p. 65, 2012.

[12] H. I. Krebs, J. J. Palazzolo, L. Dipietro, M. Ferraro, J. Krol, K. Rannekleiv, B. T. Volpe, and N. Hogan, "Rehabilitation robotics: Performance-based progressive robot-assisted therapy," *Autonomous Robots*, vol. 15, no. 1, pp. 7–20, 2003.

[13] L. Peternel, N. Tsagarakis, and A. Ajoudani, "A human–robot co-manipulation approach based on human sensorimotor information," *IEEE Transactions on Neural Systems and Rehabilitation Engineering*, vol. 25, no. 7, pp. 811–822, 2017.

[14] L. Bi, C. Guan *et al.*, "A review on emg-based motor intention prediction of continuous human upper limb motion for human-robot collaboration," *Biomedical Signal Processing and Control*, vol. 51, pp. 113–127, 2019.

[15] W. Kim, P. Balatti, E. Lamon, and A. Ajoudani, "MOCA-MAN: A MObile and reconfigurable Collaborative Robot Assistant for conjoined huMAN-robot actions," in *IEEE International Conference on Robotics and Automation (ICRA)*, 2020.

[16] E. Rocon, J. M. Belda-Lois, A. F. Ruiz, M. Manto, J. C. Moreno, and J. L. Pons, "Design and validation of a rehabilitation robotic exoskeleton for tremor assessment and suppression," *IEEE Transactions on Neural Systems and Rehabilitation Engineering*, vol. 15, no. 3, pp. 367–378, 2007.

[17] M. Lazzaroni, S. Toxiri, D. G. Caldwell, S. Anastasi, L. Monica, E. De Momi, and J. Ortiz, "Acceleration-based assistive strategy to control a back-support exoskeleton for load handling: Preliminary evaluation," in *2019 IEEE 16th International Conference on Rehabilitation Robotics (ICORR)*, 2019, pp. 625–630.

[18] C. N. Schabowsky, S. B. Godfrey, R. J. Holley, and P. S. Lum, "Development and pilot testing of hexorr: Hand exoskeleton rehabilitation robot," *Journal of NeuroEngineering and Rehabilitation*, vol. 7, no. 1, p. 36, 2010.

[19] E. Pezent, C. G. Rose, A. D. Deshpande, and M. K. O'Malley, "Design and characterization of the openwrist: A robotic wrist exoskeleton for coordinated hand-wrist rehabilitation," in *IEEE International Conference on Rehabilitation Robotics (ICORR)*, 2017, pp. 720–725.

[20] B. Sheng, S. Xie, L. Tang, C. Deng, and Y. Zhang, "An industrial robot-based rehabilitation system for bilateral exercises," *IEEE Access*, vol. 7, pp. 151 282–151 294, 2019.

[21] P. Balatti, F. Fusaro, N. Villa, E. Lamon, and A. Ajoudani, "A collaborative robotic approach to autonomous pallet jack transportation and positioning," *IEEE Access*, vol. 8, pp. 142 191–142 204, 2020.
[22] E. Lamon, F. Fusaro, P. Balatti, W. Kim, and A. Ajoudani, "A visuo-haptic guidance interface for mobile collaborative robotic assistant (moca)," in *IEEE/RSJ International Conference on Intelligent Robots and Systems (IROS)*, 2020.
[23] P. Araujo-Gómez, V. Mata, M. Díaz-Rodríguez, A. Valera, and A. Page, "Design and kinematic analysis of a novel 3ups/rpu parallel kinematic mechanism with 2t2r motion for knee diagnosis and rehabilitation tasks," *Journal of Mechanisms and Robotics*, vol. 9, no. 6, 2017.
[24] M. Abbasi and A. Afsharfard, "Modeling and experimental study of a hand tremor suppression system," *Mechanism and Machine Theory*, vol. 126, pp. 189–200, 2018.
[25] M. Vallés, J. Cazalilla, A. Valera, V. Mata, A. Page, and M. Díaz-Rodríguez, "A 3-PRS parallel manipulator for ankle rehabilitation: towards a low-cost robotic rehabilitation," *Robotica*, vol. 35, no. 10, p. 1939–1957, 2017.
[26] Z. Cao, G. Hidalgo Martinez, T. Simon, S. Wei, and Y. A. Sheikh, "OpenPose: Realtime Multi-Person 2D Pose Estimation using Part Affinity Fields," *IEEE Transactions on Pattern Analysis and Machine Intelligence*, 2019.
[27] W. Ren, O. Ma, H. Ji, and X. Liu, "Human posture recognition using a hybrid of fuzzy logic and machine learning approaches," *IEEE Access*, vol. 8, pp. 135 628–135 639, 2020.
[28] A. Lioulemes, M. Theofanidis, V. Kanal, K. Tsiakas, M. Abujelala, C. Collander, W. B. Townsend, A. Boisselle, and F. Makedon, "MAGNI dynamics: A vision-based kinematic and dynamic upper-limb model for intelligent robotic rehabilitation," *International Journal of Biomedical and Biological Engineering*, vol. 11, no. 4, pp. 158 – 167, 2017.
[29] G. Airò Farulla, D. Pianu, M. Cempini, M. Cortese, L. Russo, M. Indaco, R. Nerino, A. Chimienti, C. Oddo, and N. Vitiello, "Vision-based pose estimation for robot-mediated hand telerehabilitation," *Sensors*, vol. 16, no. 2, p. 208, 2016.
[30] D. Phan, B. Kashyap, P. N. Pathirana, and A. Seneviratne, "A constrained nonlinear optimization solution for 3d orientation estimation of the human limb," in *IEEE Biomedical Engineering International Conference (BMEiCON)*, 2017, pp. 1–4.
[31] A. Atrsaei, H. Salarieh, and A. Alasty, "Human Arm Motion Tracking by Orientation-Based Fusion of Inertial Sensors and Kinect Using Unscented Kalman Filter," *Journal of Biomechanical Engineering*, vol. 138, no. 9, 2016.
[32] F. Just, Ö. Özen, S. Tortora, V. Klamroth-Marganska, R. Riener, and G. Rauter, "Human arm weight compensation in rehabilitation robotics: efficacy of three distinct methods," *Journal of neuroengineering and rehabilitation*, vol. 17, no. 1, pp. 1–17, 2020.
[33] M. Laitenberger, M. Raison, D. Périé, and M. Begon, "Refinement of the upper limb joint kinematics and dynamics using a subject-specific closed-loop forearm model," *Multibody System Dynamics*, vol. 33, no. 4, pp. 413–438, 2015.
[34] J. M. Gandarias, J. M. Gómez-de Gabriel, and A. J. García-Cerezo, "Enhancing perception with tactile object recognition in adaptive grippers for human–robot interaction," *Sensors*, vol. 18, no. 3, 2018.
[35] L. Liu, J. Ma, Y. Luo, and H. Wu, "Mechanism design and kinematics analysis of multifunctional waist rehabilitation bed," *Vibroengineering PROCEDIA*, vol. 22, pp. 194–199, mar 2019. [Online]. Available: https://doi.org/10.21595%2Fvp.2019.20539
[36] P. Piraintorn and V. Sa-ing, "Stroke rehabilitation based on intelligence interaction system," in *2020 17th International Conference on Electrical Engineering/Electronics, Computer, Telecommunications and Information Technology (ECTI-CON)*, 2020, pp. 648–651.
[37] Y. Ren, Y. N. Wu, C. Y. Yang, T. Xu, R. L. Harvey, and L. Q. Zhang, "Developing a wearable ankle rehabilitation robotic device for in-bed acute stroke rehabilitation," *IEEE Transactions on Neural Systems and Rehabilitation Engineering*, vol. 25, no. 6, pp. 589–596, 2017.
[38] J. R. Medina, T. Lorenz, and S. Hirche, "Considering human behavior uncertainty and disagreements in human–robot cooperative manipulation," in *Trends in Control and Decision-Making for Human–Robot Collaboration Systems*, Y. Wang and F. Zhang, Eds. Cham, Germany: Springer International Publishing, 2017, pp. 207–240.
[39] G. Averta, D. Caporale, C. Della Santina, A. Bicchi, and M. Bianchi, "A technical framework for human-like motion generation with autonomous anthropomorphic redundant manipulators," in *IEEE International Conference on Robotics and Automation (ICRA)*, 2020.
[40] J. M. Gómez-de Gabriel, J. M. Gandarias, F. J. Pérez-Maldonado, F. J. García-Núñez, E. J. Fernández-García, and A. J. García-Cerezo, "Methods for autonomous wristband placement with a search-and-rescue aerial manipulator," in *IEEE/RSJ International Conference on Intelligent Robots and Systems (IROS)*, 2018, pp. 7838–7844.
[41] F. Ozkul and D. E. Barkana, "Upper-extremity rehabilitation robot rehabroby: methodology, design, usability and validation," *International Journal of Advanced Robotic Systems*, vol. 10, no. 12, p. 401, 2013.
[42] R. O. Duda and P. E. Hart, "Use of the hough transformation to detect lines and curves in pictures," *Communications of the ACM*, vol. 15, no. 1, pp. 11–15, 1972.
[43] Seul Jung, T. C. Hsia, and R. G. Bonitz, "Force tracking impedance control of robot manipulators under unknown environment," *IEEE Transactions on Control Systems Technology*, vol. 12, no. 3, pp. 474–483, 2004.
[44] O. Khatib, "A unified approach for motion and force control of robot manipulators: The operational space formulation," *IEEE Journal on Robotics and Automation*, vol. 3, no. 1, pp. 43–53, 1987.
[45] F. Ficuciello, A. Romano, L. Villani, and B. Siciliano, "Cartesian impedance control of redundant manipulators for human-robot comanipulation," in *2014 IEEE/RSJ International Conference on Intelligent Robots and Systems*, 2014, pp. 2120–2125.
[46] C. Ott, *Cartesian impedance control of redundant and flexible-joint robots*. Springer, 2008.
[47] A. Albu-Schaffer, C. Ott, U. Frese, and G. Hirzinger, "Cartesian impedance control of redundant robots: recent results with the dlr-light-weight-arms," in *IEEE International Conference on Robotics and Automation (ICRA)*, vol. 3, 2003, pp. 3704–3709 vol.3.
[48] S. Chatterjee and A. S. Hadi, *Regression analysis by example*. John Wiley & Sons, 2015.
[49] J. Illingworth and J. Kittler, "A survey of the hough transform," *Computer vision, graphics, and image processing*, vol. 44, no. 1, pp. 87–116, 1988.
[50] M. Gautier and P. Poignet, "Extended kalman filtering and weighted least squares dynamic identification of robot," *Control Engineering Practice*, vol. 9, no. 12, pp. 1361–1372, 2001. [Online]. Available: https://www.sciencedirect.com/science/article/pii/S0967066101001058
[51] B. L. Bonilla and H. H. Asada, "A robot on the shoulder: Coordinated human-wearable robot control using coloured petri nets and partial least squares predictions," in *2014 IEEE International Conference on Robotics and Automation (ICRA)*, 2014, pp. 119–125.
[52] A. Wan, J. Xu, H. Chen, S. Zhang, and K. Chen, "Optimal path planning and control of assembly robots for hard-measuring easy-deformation assemblies," *IEEE/ASME Transactions on Mechatronics*, vol. 22, no. 4, pp. 1600–1609, 2017.
[53] V. Strejc, "Least squares parameter estimation," *Automatica*, vol. 16, no. 5, pp. 535–550, 1980. [Online]. Available: https://www.sciencedirect.com/science/article/pii/0005109880900771
[54] S. Boyd and L. Vandenberghe, *Introduction to applied linear algebra: vectors, matrices, and least squares*. Cambridge university press, 2018.

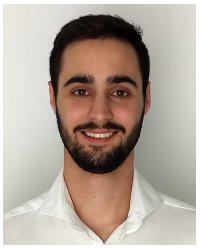

FRANCISCO J. RUIZ-RUIZ received his B.S. and M.S. degrees in mechatronics engineering from the University of Málaga, Málaga, Spain, in 2018 and 2019, respectively, and is currently pursuing a Ph.D. degree in mechatronics engineering at the University of Málaga. He is currently a Research Assistant with the Department of Systems Engineering and Automation at the University of Málaga. His research interests include pHRI, control design of robotic manipulators, and internet of things.

JUAN M. GANDARIAS is a postdoctoral researcher at the Human-Robot Interfaces and Physical Interaction lab (HRI2) at Istituto Italiano di Tecnologia (IIT). He received his B.S., M.S., and Ph.D. in Mechatronics from the University of Málaga in 2015, 2017, and 2020, respectively. He has contributed to several Spanish and European projects related to search-and-rescue, physical robotic assistance and Human-Robot Collaboration in Industrial environments. His research interests include pHRI, human modeling, and haptic perception.

FRANCISCO PASTOR received his M.Sc. degree in mechatronics engineering in 2017 from the University of Málaga, Spain. He is currently working toward the PhD degree in mechatronics engineering in the Robotics and Mechatronics Group of the University of Malaga. He has collaborated as a researcher in a project of rescue robotics and mobile robots. His current research interests include pHRI and tactile perception.

JESÚS M. GÓMEZ-DE-GABRIEL received his engineering and Ph.D. degrees in computer science from the University of Málaga, Málaga, Spain, in 1990 and 1999, respectively. He is currently an Associate Professor with the Department of Systems Engineering and Automation, University of Málaga. He has led a project on telerobotic surgery and has participated in medical robotics projects and other projects related to mobile robots and factory automation. His current research interests include pHRI, internet of things, education in engineering, and mobile robotics.